Analytical solution for the Mollow and Autler-Townes probe absorption spectra of a three-level atom in a squeezed vacuum

M. Bosticky, Z. Ficek, and B. J. Dalton
Department of Physics, The University of Queensland, Brisbane 4072, Australia
(Received 25 June 1997; revised manuscript received 16 December 1997)

The Mollow and Autler-Townes probe absorption spectra of a three-level atom in a cascade configuration with the lower transition coherently driven and also coupled to a narrow bandwidth squeezed-vacuum field are studied. Analytical studies of the modifications caused by the finite squeezed-vacuum bandwidth to the spectra are made for the case when the Rabi frequency of the driving field is much larger than the natural linewidth. The squeezed vacuum center frequency and the driving laser frequency are assumed equal. We show that the spectral features depend on the bandwidth of a squeezed vacuum field and whether the sources of the squeezing field are degenerate (DPA) or nondegenerate (NDPA) parametric amplifiers. In a broadband or narrow bandwidth squeezed vacuum generated by a NDPA, the central component of the Mollow spectrum can be significantly narrower than that in the normal vacuum. When the source of the squeezed vacuum is a DPA, the central feature is insensitive to squeezing. The Rabi sidebands, however, can be significantly narrowed only in the squeezed vacuum produced by the DPA. The two lines of the Autler-Townes absorption spectrum can be narrowed only in a narrow bandwidth squeezed vacuum, whereas they are independent of the phase and are always broadened in a broadband squeezed vacuum. [S1050-2947(98)10404-3]

PACS number(s): 42.50.Dv, 32.70.Jz

I. INTRODUCTION

Since the first paper of Gardiner [1] on the interaction of a two-level atom with a squeezed vacuum, there has been a lot of research done on the spectroscopy with squeezed light [2]. At the same time, considerable progress has been made in the developing of sources of the squeezed-vacuum field (mainly parametric amplifiers). This progress has allowed to test the novel predictions of the matter squeezed field interaction [3–5]. In the spectroscopic applications of the squeezed-vacuum field two- and three-level atoms are the favorite systems, often in free space but more recently treated in cavities. The latter has been recognized as being most suitable for an observation of the squeezed-vacuum effects as it does not require squeezing of all modes in the full 4π solid angle. Studies of modifications to spontaneous emission, resonance fluorescence, probe absorption spectra, and photon statistics are included in the topics covered.

Much of the work to date has considered broad bandwidth squeezed-vacuum fields, where the bandwidths are not only large compared to the spontaneous emission linewidth, but also larger than the Rabi frequencies and detunings of a driving field. A broad bandwidth approximation allows to develop the theory in terms of a Markovian master equation using uncoupled atom-driving field states. Recent work involving the broadband squeezed vacuum case by Swain *et al.* [6–9] has demonstrated some new, unusual features in the resonance fluorescence and probe absorption spectra [10–12], so there is still an interest in studying the broadband case.

However, the common squeezed-vacuum field sources, the parametric amplifiers [2], generate a narrow rather than broadband field. Therefore, theoretical studies of atomic spectroscopic behavior for finite bandwidth sources are of practical interest. For undriven atoms in free space, where weak coupling conditions apply, a finite bandwidth of the squeezed vacuum can decrease the potential of the line narrowing found in absorption and spontaneous emission spectra [13–16]. For coherently driven systems in a finite-bandwidth squeezed vacuum, however, the spectral linewidth can be narrower than that in a broadband squeezed vacuum [17–19]. The effects differ depending on whether the squeezed field is maximally squeezed at a central frequency (as in a degenerate parametric amplifier) or at frequencies equally displaced from a central frequency (as in a nondegenerate parametric amplifier). Work has also been carried out for an intrinsically non-Markovian case where the squeezing bandwidth is comparable or even small compared to the decay rate [20]. Numerical treatments of finite bandwidth squeezed-vacuum effects using both adjoint equations [19,14,21,20] and stochastic density matrix methods [15,16] have been carried out. Recently, an analytical dressed atom approach [17,22–28] involving Markovian master equations [29] has been proposed. This approach provides a simple understanding of the finite squeezed-vacuum effects. However, the approach is valid for squeezed vacuum bandwidths much greater than the normal vacuum decay width in order to satisfy the Markov approximation. Despite this, the approach allows to discuss the cases where the squeezed-vacuum field bandwidth is small compared to the Rabi frequencies and detunings of driving laser fields [17,28].

In a previous paper [28] (to be referred to as I), we have presented a method based on a master equation approach using dressed atom states to calculate the Mollow and Autler-Townes probe absorption spectra of a three-level cascade atom. In the calculations we assumed that one of the two atomic transitions is strongly driven by a coherent laser field and damped by a narrow bandwidth squeezed vacuum. The spectra were calculated numerically for a squeezed vacuum produced by a degenerate parametric amplifier (DPA) and the carrier frequency of the squeezed-vacuum

field equal to the driving laser field frequency. In the present paper, we present analytical solutions for the probe spectra and extend the theory to a nondegenerate parametric amplifier (NDPA) source of squeezed light. In order to get a better insight into the role of different sources of the squeezed vacuum in the spectral narrowing, we derive analytical formulas for the bandwidths of spectral features for both the DPA and NDPA cases and compare them with the broadband case. For simplicity, we restrict ourselves to the case where the squeezed-vacuum center frequencies and the driving frequency coincide.

The paper is organized as follows. In Sec. II, we briefly outline the theory, which was derived in I, and extend it to the case of a NDPA. In Sec. III, we present analytical results for the absorption spectra. Numerical results of the absorption spectra are presented in Sec. IV. In Sec. V, we compare the analytical expressions for the widths of the spectral features with the numerical results. We summarize the results in Sec. VI.

II. THEORETICAL FORMALISM

We consider a three-level atom in a cascade configuration with the upper level $|3\rangle$, the intermediate level $|2\rangle$, and the ground level $|1\rangle$ separated by the transition frequencies ω_{32} and ω_{21}, respectively. We assume that the lower 1-2 transition is driven by a strong laser field of the Rabi frequency Ω and frequency ω_a, which is detuned from the transition by $\delta=\omega_{21}-\omega_a$. In addition to the driving field, the lower transition is coupled to a squeezed-vacuum field of the phase ϕ_s and the carrier frequency ω_s. The squeezed-vacuum field detuning δ_s from the laser frequency $\delta_s=\omega_a-\omega_s$ is set to zero, however. The radiation properties of the system are analyzed by calculating absorption spectra of a probe field of frequency ω_p. The probe field is assumed weak and can be tuned to the lower transition ($\omega_p\approx\omega_{21}$) to study the Mollow absorption spectrum [30], or can be tuned to the upper transition ($\omega_p\approx\omega_{32}$) to study the Autler-Townes absorption spectrum [31].

The narrow band squeezed-vacuum case will be treated with $\Omega\gg\Gamma_s\gg\Gamma_0$ and compared with the broadband case, where $\Gamma_s\gg\Omega,\Gamma_0$. Γ_s is the squeezed vacuum bandwidth and Γ_0 is the spontaneous decay rate for the 1-2 transition. The squeezed-vacuum field source is assumed to be either a DPA or NDPA, whose output is characterized by the following correlation functions [32]:

$$\langle a_k^\dagger a_l\rangle=N(\omega_l)\quad\text{if}\quad\omega_k=\omega_l,$$
$$=0\quad\text{otherwise}\tag{2.1}$$

and

$$\langle a_k a_l\rangle=M(\omega_l)\quad\text{if}\quad\omega_k+\omega_l=2\omega_s,$$
$$=0\quad\text{otherwise},\tag{2.2}$$

where $N(\omega_l)$ and $M(\omega_l)$ are squeezing parameters giving the photon number and two photon correlation functions, respectively. For the DPA source they are given by [33,34]

$$N(\omega_l)=\frac{b_y^2-b_x^2}{4}\left\{\frac{1}{(\omega_l-\omega_a)^2+b_x^2}-\frac{1}{(\omega_l-\omega_a)^2+b_y^2}\right\},$$
$$M(\omega_l)=-e^{i\phi_s}\frac{b_y^2-b_x^2}{4}\left\{\frac{1}{(\omega_l-\omega_a)^2+b_x^2}+\frac{1}{(\omega_l-\omega_a)^2+b_y^2}\right\},\tag{2.3}$$

and for the NDPA source [32,34]

$$N(\omega_l)=\frac{b_y^2-b_x^2}{4}\left\{\frac{1}{(\omega_l-\omega_a+\alpha)^2+b_x^2}+\frac{1}{(\omega_l-\omega_a-\alpha)^2+b_x^2}-\frac{1}{(\omega_l-\omega_a+\alpha)^2+b_y^2}-\frac{1}{(\omega_l-\omega_a-\alpha)^2+b_y^2}\right\},$$
$$M(\omega_l)=-e^{i\phi_s}\frac{b_y^2-b_x^2}{4}\left\{\frac{1}{(\omega_l-\omega_a+\alpha)^2+b_x^2}+\frac{1}{(\omega_l-\omega_a-\alpha)^2+b_x^2}+\frac{1}{(\omega_l-\omega_a+\alpha)^2+b_y^2}+\frac{1}{(\omega_l-\omega_a-\alpha)^2+b_y^2}\right\},\tag{2.4}$$

with

$$b_x=\frac{\gamma_c}{2}-\epsilon,$$
$$b_y=\frac{\gamma_c}{2}+\epsilon.\tag{2.5}$$

The parameters γ_c and ϵ are the cavity decay rate and the amplification constant of the parametric amplifier, respectively. The squeezed-vacuum spectrum of the DPA source has one peak centered at ω_a, whereas the squeezed-vacuum spectrum of the NDPA source has two peaks centered at ω_a and separated from the central frequency by $\pm\alpha$. The squeezing bandwidth Γ_s can be taken equal to b_x, the smaller of the two linewidth factors. The peak heights for the DPA and NDPA curves have been made the same in order to compare the results.

In our paper (I), we have derived a Markovian master equation for the reduced atomic density operator ρ_A [see Eq. (2.47) of I]. In terms of the semiclassical dressed states, the master equation can be written as

$$\frac{\partial\rho_A}{\partial t}=\frac{1}{i\hbar}[\tilde{H}_A,\rho_A]+\sum_{i,j}\Gamma_{ij}([\tilde{T}_j\rho_A,\tilde{T}_i]+[\tilde{T}_j,\rho_A\tilde{T}_i]),\tag{2.6}$$

where Γ_{ij} are the dressed-atom relaxation rates based on secular approximations [see Eqs. (2.48) and (2.50) of I],

$$\tilde{T}_1=\frac{1}{2}(|\tilde{2}\rangle\langle\tilde{2}|-|\tilde{1}\rangle\langle\tilde{1}|),$$
$$\tilde{T}_2=\tilde{T}_3^\dagger=|\tilde{2}\rangle\langle\tilde{1}|,$$

$$\widetilde{T}_4=\frac{1}{2}(|\widetilde{2}\rangle\langle\widetilde{2}|+|\widetilde{1}\rangle\langle\widetilde{1}|),$$

$$\widetilde{T}_5=\widetilde{T}^{\dagger}_7=|\widetilde{3}\rangle\langle\widetilde{1}|, \tag{2.7}$$

$$\widetilde{T}_6=\widetilde{T}^{\dagger}_8=|\widetilde{3}\rangle\langle\widetilde{2}|,$$

$$\widetilde{T}_9=|\widetilde{3}\rangle\langle\widetilde{3}|,$$

are the atomic operators given in terms of the semiclassical dressed states

$$|\widetilde{1}\rangle=\cos(\theta)|1\rangle+i\ \sin(\theta)e^{-i(\omega_a t+\phi_a)}|2\rangle,$$

$$|\widetilde{2}\rangle=i\ \sin(\theta)|1\rangle+\cos(\theta)e^{-i(\omega_a t+\phi_a)}|2\rangle, \tag{2.8}$$

$$|\widetilde{3}\rangle=e^{-i(\omega_a t+\phi_a)}|3\rangle,$$

with

$$\tan(\theta)=\frac{-\delta+\Omega'}{\Omega}, \tag{2.9}$$

and

$$\Omega'=\sqrt{\delta^2+\Omega^2}. \tag{2.10}$$

In Eq. (2.6), $\widetilde{H}_A$ is the dressed-atom Hamiltonian defined as

$$\widetilde{H}_A=\sum_{\alpha=1}^{3}\hbar\nu_\alpha|\widetilde{\alpha}\rangle\langle\widetilde{\alpha}|, \tag{2.11}$$

where

$$\nu_1=(\delta-\Omega')/2,$$

$$\nu_2=(\delta+\Omega')/2, \tag{2.12}$$

$$\nu_3=\omega_{32}+\delta$$

are the detunings of the dressed-atom frequencies from the driving laser frequency ω_a. The sum in Eq. (2.6) is over $i,j=\{1,2,3,5,6,7,8\}$ and certain frequency shift terms have been ignored.

Having available the master equation of the system, we can derive the equations of motion for the expectation values of the dressed-atom operators (2.7). The set of the equations can be written in a matrix form as

$$\frac{d\mathbf{T}}{dt}=\mathbf{H}\cdot\mathbf{T}, \tag{2.13}$$

where $\mathbf{T}=(\langle\widetilde{T}_1\rangle,\langle\widetilde{T}_2\rangle,\ldots,\langle\widetilde{T}_9\rangle)$ is a column vector, and $\mathbf{H}$ is a 9×9 matrix whose elements H_{ij} are given in Eqs. (3.8) and (3.9) of I. As before, certain frequency shift terms $\widetilde{\Delta}_N(\omega_i)$ are ignored. The matrix elements H_{ij} depend on the detuning δ, the Rabi frequency Ω, and on relaxation terms $\widetilde{M}(\omega_i)$ and $\widetilde{\Gamma}_N(\omega_i)$ [see Eqs. (3.3) and (3.6) of I] induced by the squeezed vacuum and evaluated at the dressed-atom transition frequencies

$$\omega_1=\omega_a,$$

$$\omega_2=\omega_a+\Omega', \tag{2.14}$$

$$\omega_3=\omega_a-\Omega'.$$

Using contour integral methods, we find the explicit form of the relaxation terms, which for the DPA are

$$\widetilde{M}(\omega_i)=\frac{\Gamma_0}{8}e^{i\phi_s}\frac{b_y^2-b_x^2}{b_x b_y}\times\frac{[-i(\omega_a-\omega_i)(b_y+b_x)+(b_y^2+b_x^2)]}{[(\omega_a-\omega_i+ib_x)(\omega_a-\omega_i+ib_y)]},$$

$$\widetilde{\Gamma}_N(\omega_i)=[1+2N(\omega_i)]\Gamma_0, \tag{2.15}$$

where $N(\omega_i)$ is given in Eq. (2.3). For the NDPA the relaxation terms are given by

$$\widetilde{M}(\omega_i)=-\frac{\Gamma_0}{2}e^{i\phi_s}\frac{b_y^2-b_x^2}{8}\left\{\frac{i(\omega_a-\omega_i+\alpha)+b_x}{(\omega_a-\omega_i+\alpha)^2+b_x^2}\frac{1}{b_x}+\frac{i(\omega_a-\omega_i+\alpha)+b_y}{(\omega_a-\omega_i+\alpha)^2+b_y^2}\frac{1}{b_y}+\frac{i(\omega_a-\omega_i-\alpha)+b_x}{(\omega_a-\omega_i-\alpha)^2+b_x^2}\frac{1}{b_x}+\frac{i(\omega_a-\omega_i-\alpha)+b_y}{(\omega_a-\omega_i-\alpha)^2+b_y^2}\frac{1}{b_y}\right\}, \tag{2.16}$$

$$\widetilde{\Gamma}_N(\omega_i)=[1+2N(\omega_i)]\Gamma_0, \tag{2.17}$$

where Γ_0 is the spontaneous emission rate of the 2-1 transition. The squeezing modified relaxation rates $\widetilde{M}(\omega_i)$ and $\widetilde{\Gamma}_N(\omega_i)$ can have different values depending on the frequency ω_i about which they are evaluated. For the DPA source and $\Omega'\gg b_x,b_y$, the squeezing vacuum appears only around the central frequency and then the relaxation terms reduce to

$$\widetilde{M}(\omega_1)=-\frac{1}{2}\Gamma_0 M e^{i\phi_s},\quad \widetilde{M}(\omega_2)=\widetilde{M}(\omega_3)=0,$$

$$\widetilde{\Gamma}_N(\omega_1)=(1+2N)\Gamma_0,\quad \widetilde{\Gamma}_N(\omega_2)=\widetilde{\Gamma}_N(\omega_3)=\Gamma_0, \tag{2.18}$$

where N and $M=\sqrt{N(N+1)}$ denote, respectively, the magnitudes of the photon number $N(\omega_i)$ and the two-photon correlations $M(\omega_i)$ evaluated at their peaks. For the NDPA source with $\alpha=\Omega'$, the two peaks couple to the side frequencies ω_2 and ω_3 and in this case the relaxation terms are

$$\widetilde{M}(\omega_1)=0,\quad \widetilde{M}(\omega_2)=\widetilde{M}(\omega_3)=-\frac{1}{2}\Gamma_0 M e^{i\phi_s},$$

$$\widetilde{\Gamma}_N(\omega_1)=0,\quad \widetilde{\Gamma}_N(\omega_2)=\widetilde{\Gamma}_N(\omega_3)=(1+2N)\Gamma_0. \tag{2.19}$$

The set of Eqs. (2.13) with the relaxation terms (2.18) and (2.19) together with the quantum regression theorem [35] allow us to calculate both the Mollow and Autler-Townes probe absorption spectra.

III. ANALYTICAL CALCULATION OF THE ABSORPTION SPECTRA

The atomic transitions, the lower driven by a laser field and coupled to a finite bandwidth squeezed vacuum and the upper undriven transition, can be monitored by a weak probe beam. For the probe beam coupled to the driven transition, the Mollow absorption spectrum can be evaluated, whereas for the probe coupled to the upper 2-3 transition the Autler-Townes spectrum can be studied. In the limit of a strong driving field, $\Omega \gg \Gamma_0$, approximate forms of the spectra can be obtained. The probe frequency ω_p can be expressed in terms of a small detuning $\delta\omega$ from any particular resonant feature of interest. The Mollow probe absorption spectra about any feature can be approximately found by application of Taylor's series with respect to small quantities such as $\delta\omega/\Omega'$. For the Autler-Townes probe absorption spectrum, the same approach can be applied to obtain the approximate analytical results. We will consider the case where $\delta_s = \omega_a - \omega_s$ is zero.

In our model only the lower transition of the three-level atom is driven by a laser field and coupled to a squeezed vacuum. For simplicity, the upper level 3 is treated as a spectator only, in that relaxation rates associated with the 2-3 transitions are ignored in comparison with those for the 1-2 transition. In this case we can separate the dynamics of the lower transition from that of the upper transition. Therefore, we can approximately treat the lower transition as an individual two-level system. In order to find the dynamics of this system it is enough to determine the time evolution of the one time averages of only three dressed operators $\langle \tilde{T}_1 \rangle$, $\langle \tilde{T}_2 \rangle$, and $\langle \tilde{T}_3 \rangle$. The equations of motion for these operators are easily subtracted from Eq. (2.13), and for $\Omega' \gg \Gamma_0$ can be written in a matrix form as

$$\frac{d\mathbf{T}_m}{dt} = \mathbf{H}_m \cdot \mathbf{T}_m, \tag{3.1}$$

where $\mathbf{T}_m = (\langle \tilde{T}_1 \rangle, \langle \tilde{T}_2 \rangle, \langle \tilde{T}_3 \rangle)$, and

$$\mathbf{H}_m = \begin{pmatrix} -H_1 & H_2 & H_2^* \\ H_3 & -H_4 + i\tilde{\Omega}' & H_5 \\ H_3^* & H_5^* & -H_4 - i\tilde{\Omega}' \end{pmatrix}, \tag{3.2}$$

with

$$\begin{aligned}
H_1 &= 4D_2D_3[|\tilde{M}(\omega_2)| + |\tilde{M}(\omega_3)|]\cos\phi + D_2^2\tilde{\Gamma}_N(\omega_2) \\
&\quad + D_3^2\tilde{\Gamma}_N(\omega_3), \\
H_2 &= D_1|\tilde{M}(\omega_1)|(D_2 e^{i\phi} - D_3 e^{-i\phi}) \\
&\quad - \frac{1}{4}D_1(D_2 - D_3)\tilde{\Gamma}_N(\omega_1), \\
H_3 &= 2D_1[D_3 e^{i\phi}|\tilde{M}(\omega_3)| - D_2 e^{-i\phi}|\tilde{M}(\omega_2)|] \\
&\quad + \frac{1}{2}D_1[D_2\tilde{\Gamma}_N(\omega_2) - D_3\tilde{\Gamma}_N(\omega_3)], \\
H_4 &= 2D_1^2|\tilde{M}(\omega_1)|\cos\phi \\
&\quad + 2D_2D_3[|\tilde{M}(\omega_2)| + |\tilde{M}(\omega_3)|]\cos\phi \\
&\quad + \frac{1}{2}[-D_1^2\tilde{\Gamma}_N(\omega_1) + D_2^2\tilde{\Gamma}_N(\omega_2) + D_3^2\tilde{\Gamma}_N(\omega_3)], \\
H_5 &= 2D_3^2 e^{i\phi}|\tilde{M}(\omega_3)| + 2D_2^2 e^{-i\phi}|\tilde{M}(\omega_2)| \\
&\quad + \frac{1}{2}D_2D_3[\tilde{\Gamma}_N(\omega_2) + \tilde{\Gamma}_N(\omega_3)], \\
\tilde{\Omega}' &= \Omega' - 2D_2D_3(|\tilde{M}(\omega_2)| - |\tilde{M}(\omega_3)|)\sin\phi,
\end{aligned} \tag{3.3}$$

and $\phi = 2\phi_a + \phi_s$. The coefficients (3.3) are obtained from Eq. (3.8) of I after ignoring the shift parameters $\tilde{\Delta}_N(\omega_i)$, which are very small for $\Omega' \gg \Gamma_0, b_x, b_y$. The quantities D_i are given in terms of the tipping angle θ as

$$\begin{aligned}
D_1 &= 2i\,\sin\theta\cos\theta, \\
D_2 &= \sin^2\theta, \\
D_3 &= \cos^2\theta, \\
D_5 &= i\,\sin\theta, \\
D_6 &= \cos\theta.
\end{aligned} \tag{3.4}$$

Applying the quantum regression theorem [35] to obtain the two time averages from Eq. (3.1) for the one time averages and using Laplace transform methods, we find that for $\Omega' \gg \Gamma_0$ the stationary Mollow spectrum can be written as

$$S^m(\omega_p, \infty) = \frac{1}{\mathcal{N}_m}\mathrm{Re}\left\{ \frac{A_2(s)}{(s+H_1)(s+H_4+i\tilde{\Omega}')(s+H_4-i\tilde{\Omega}')} \right\}_{s=-i\delta\omega_p}, \tag{3.5}$$

where $\mathcal{N}_m$ is the normalization constant given in terms of the stationary value $\langle \tilde{T}_i \rangle_s$ of the dressed operators as

$$\mathcal{N}_m = 2\pi \langle \tilde{T}_1 \rangle_s (D_3 - D_2) + \pi D_1 (\langle \tilde{T}_3 \rangle_s - \langle \tilde{T}_2 \rangle_s), \quad (3.6)$$

and $A_2(s)$ is a second order polynomial in s. The parameter $\delta\omega_p$ is the probe detuning from the laser frequency ($\delta\omega_p$ ($\delta\omega$p$=\omega_p-\omega_a$). We note from Eq. (3.5) that the denominator has three minima, the central at $\delta\omega_p=0$, and two sidebands at $\delta\omega_p=\pm\tilde{\Omega}'$. These minima correspond to the three features of the Mollow triplet.

It is interesting to note that the Rabi sidebands of the Mollow spectrum are located at $\pm\tilde{\Omega}'$, which are shifted from Ω' by $2D_2D_3[|\tilde{M}(\omega_2)|-|\tilde{M}(\omega_3)|]\sin\phi$ [see Eq. (3.3)]. The shift appears only for a narrow bandwidth squeezed bandwidth with $\phi=\pi/2$, and $\tilde{M}(\omega_2)\neq\tilde{M}(\omega_3)$. Therefore, in order to observe the shift, the squeezing spectrum should be asymmetric about ω_s.

At the central feature we can write $\delta\omega_p=\delta\omega$, where $\delta\omega$ is the probe detuning from the central frequency ω_a, and then for $\Omega' \gg H_4$ the Mollow probe absorption spectrum can be approximately written as

$$S_C^m(\delta\omega,\infty) \approx \frac{1}{\mathcal{N}_m}\mathrm{Re}\left\{ B_c + \frac{-(A_c+B_cH_1)H_1}{\delta\omega^2+H_1^2} + \frac{i(A_c+B_cH_1)\delta\omega}{\delta\omega^2+H_1^2}\right\}, \quad (3.7)$$

where

$$\begin{aligned} A_c \approx & -D_1(D_2\langle\tilde{T}_2\rangle_s - D_3\langle\tilde{T}_3\rangle_s) \\ & + i\frac{1}{\Omega'}\{-2H_1\langle\tilde{T}_1\rangle_s(D_2^2+D_3^2) \\ & -2\langle\tilde{T}_1\rangle_s D_1(D_3H_2+D_2H_2^*) + D_1H_1(D_3\langle\tilde{T}_2\rangle_s \\ & + D_2\langle\tilde{T}_3\rangle_s) + D_1^2(H_2\langle\tilde{T}_2\rangle_s + H_2^*\langle\tilde{T}_3\rangle_s) \\ & + D_2D_3(H_3\langle\tilde{T}_2\rangle_s + H_3^*\langle\tilde{T}_3\rangle_s) - (D_3^2H_3\langle\tilde{T}_3\rangle_s \\ & + D_2^2H_3^*\langle\tilde{T}_2\rangle_s)\} \end{aligned} \quad (3.8)$$

and

$$B_c \approx i\frac{1}{\Omega'}\{2\langle\tilde{T}_1\rangle_s(D_2^2+D_3^2) - D_1(D_3\langle\tilde{T}_2\rangle_s + D_2\langle\tilde{T}_3\rangle_s)\}. \quad (3.9)$$

In the parameter A_c, the approximation was taken to the order of $1/\Omega'$ since the first term, which is typically of zero order in $1/\Omega'$, can be very small and then terms of the order $1/\Omega'$ can dominate. In the parameter B_c the first nonvanishing term is of order $1/\Omega'$.

The first term in the spectrum (3.7) is the vertical shift of the central feature. The second term corresponds to the Lorentzian absorption part of the spectra and the third to the Rayleigh dispersion part.

For the left feature at $\delta\omega_p \approx -\Omega'$, we can write $\delta\omega_p = \delta\omega - \Omega'$, where $\delta\omega$ is a small detuning about the left feature, and then the spectrum (3.5) reduces to

$$S_L^m(\delta\omega,\infty) \approx \frac{1}{\mathcal{N}_m}\mathrm{Re}\left\{ \frac{-A_LH_4}{\delta\omega^2+H_4^2} + \frac{iA_L\delta\omega}{\delta\omega^2+H_4^2}\right\}, \quad (3.10)$$

where $A_L = D_3(2D_3\langle\tilde{T}_1\rangle_s - D_1\langle\tilde{T}_2\rangle_s)$. The left-hand side feature of the absorption spectrum is composed of the Lorentzian and Rayleigh components, respectively.

Similarly, we can show that the right feature of the Mollow probe absorption spectra at $\delta\omega_p \approx \Omega'$ is given by

$$S_R^m(\delta\omega,\infty) \approx \frac{1}{\mathcal{N}_m}\mathrm{Re}\left\{ \frac{-A_RH_4}{\delta\omega^2+H_4^2} + \frac{iA_R\delta\omega}{\delta\omega^2+H_4^2}\right\}, \quad (3.11)$$

where $A_R = -D_2(2D_2\langle\tilde{T}_1\rangle_s - D_1\langle\tilde{T}_3\rangle_s)$ and now $\delta\omega_p = \delta\omega + \Omega'$.

The dynamics of the upper 2-3 transition are determined by two dressed operators $\tilde{T}_7$ and $\tilde{T}_8$. For $\Omega' \gg \Gamma_0$ the equations of motion for these operators can be easily subtracted from Eq. (2.13) and can be written as

$$\frac{d\mathbf{T}_a}{dt} = \mathbf{H}_a \cdot \mathbf{T}_a, \quad (3.12)$$

where $\mathbf{T}_a = \{\langle\tilde{T}_7\rangle, \langle\tilde{T}_8\rangle\}$, and

$$\mathbf{H}_a = \begin{pmatrix} -H_6 - i(\delta+\Omega')/2 & H_7 \\ H_8 & -H_9 - i(\delta-\Omega')/2 \end{pmatrix}, \quad (3.13)$$

with

$$\begin{aligned} H_6 = & \frac{1}{2}D_1^2|\tilde{M}(\omega_1)|\cos\phi + D_2D_3[|\tilde{M}(\omega_3)|e^{i\phi} + |\tilde{M}^*(\omega_2)|e^{-i\phi}] - \frac{1}{8}D_1^2\tilde{\Gamma}_N(\omega_1) + \frac{1}{4}D_2^2[\tilde{\Gamma}_N(\omega_2) \\ & - \tilde{\Gamma}_0(\omega_2)] + \frac{1}{4}D_3^2[\tilde{\Gamma}_N(\omega_3) + \tilde{\Gamma}_0(\omega_3)], \\ H_7 = & -\frac{1}{4}D_1\Gamma_0 + \frac{1}{8}D_1\{D_2[\tilde{\Gamma}_N(\omega_1) - \tilde{\Gamma}_N(\omega_2)] - D_3[\tilde{\Gamma}_N(\omega_1) - \tilde{\Gamma}_N(\omega_3)]\} \\ & - \frac{1}{2}D_1D_2[|\tilde{M}(\omega_1)| - |\tilde{M}(\omega_2)|]e^{i\phi} + \frac{1}{2}D_1D_3[|\tilde{M}^*(\omega_1)| - |\tilde{M}^*(\omega_3)|]e^{-i\phi}, \end{aligned}$$

$$H_8=\frac{1}{4}D_1\Gamma_0+\frac{1}{8}D_1\{D_2[\tilde{\Gamma}_N(\omega_1)-\tilde{\Gamma}_N(\omega_2)]-D_3[\tilde{\Gamma}_N(\omega_1)-\tilde{\Gamma}_N(\omega_3)]\}$$
$$-\frac{1}{2}D_1D_2[|\tilde{M}^*(\omega_1)|-|\tilde{M}^*(\omega_2)|]e^{-i\phi}+\frac{1}{2}D_1D_3[|\tilde{M}(\omega_1)|-|\tilde{M}(\omega_3)|]e^{i\phi}, \tag{3.14}$$

$$H_9=\frac{1}{2}D_1^2|\tilde{M}(\omega_1)|\cos\phi+D_2D_3[|\tilde{M}(\omega_2)|e^{i\phi}+|\tilde{M}^*(\omega_3)|e^{-i\phi}]-\frac{1}{8}D_1^2\tilde{\Gamma}_N(\omega_1)$$
$$+\frac{1}{4}D_2^2[\tilde{\Gamma}_N(\omega_2)+\tilde{\Gamma}_0(\omega_2)]+\frac{1}{4}D_3^2[\tilde{\Gamma}_N(\omega_3)-\tilde{\Gamma}_0(\omega_3)].$$

Using the quantum regression theorem to obtain the two time averages from Eq. (3.12) for the one time averages and using Laplace transform, we find that for $\delta_s=0$ and $\Omega'\gg\Gamma_0$ the Autler-Townes spectrum can be written as

$$S^A(\omega_p,\infty)=\frac{1}{\mathcal{N}_m}\mathrm{Re}\left\{\frac{A_1(s)}{[s+H_6+i(\Omega'+\delta)/2][s+H_9-i(\Omega'-\delta)/2]}\right\}_{s=-i\delta\omega_p'}, \tag{3.15}$$

where $\mathcal{N}_{AT}$ is the normalization constant

$$\mathcal{N}_{AT}=\pi\left[\frac{1}{2}+(D_5^2+D_6^2)\langle\tilde{T}_1\rangle_s+D_5D_6(\langle\tilde{T}_2\rangle_s-\langle\tilde{T}_3\rangle_s)\right], \tag{3.16}$$

and $A_1(s)$ is a first order polynomial in s given by the numerator of Eq. (2.83) of I times the determinant of $(sE_2-H'_{(2\times2)})$. In Eq. (3.15), $\delta\omega_p'$ is the probe detuning from the upper transition frequency of the atom given by $\delta\omega_p'=\omega_p-\omega_{32}$.

The spectrum is composed of two lines located at $-(\Omega'-\delta)/2$ and $(\Omega'+\delta)/2$. Near the left feature we can write $\delta\omega_p'=-(\Omega'-\delta)/2+\delta\omega$, where $\delta\omega$ is the detuning of the probe frequency from the center of the line. Thus at the left feature, we can approximate Eq. (3.15) to

$$S_L^A(\delta\omega,\infty)\approx\frac{1}{\mathcal{N}_{AT}}\mathrm{Re}\left\{\frac{H_9A_L}{\delta\omega^2+H_9^2}-i\frac{A_L\delta\omega}{\delta\omega^2+H_9^2}\right\}, \tag{3.17}$$

where

$$A_L=D_5^2\left(\frac{1}{2}-\langle\tilde{T}_1\rangle_s\right)+D_5D_6\langle\tilde{T}_2\rangle_s. \tag{3.18}$$

In the Autler-Townes probe absorption spectra the Lorentzian features dominate. Thus dropping the Rayleigh part of the spectrum and taking the real part of A_L we have

$$S_L^A(\delta\omega,\infty)\approx\frac{1}{\mathcal{N}_{AT}}\frac{H_9\mathrm{Re}\{A_L\}}{\delta\omega^2+H_9^2}, \tag{3.19}$$

where

$$\mathrm{Re}\{A_L\}=D_5^2\left(\frac{1}{2}-\langle\tilde{T}_1\rangle_s\right)+D_5D_6(\langle\tilde{T}_2\rangle_s-\langle\tilde{T}_3\rangle_s)/2. \tag{3.20}$$

For the right feature the absorption spectra are centered at frequency $\omega_{32}+(\Omega'+\delta)/2$ and similarly to the left feature is given by

$$S_R^A(\delta\omega,\infty)\approx\frac{1}{\mathcal{N}_{AT}}\frac{H_6\mathrm{Re}\{A_R\}}{\delta\omega^2+H_6^2}, \tag{3.21}$$

where

$$\mathrm{Re}\{A_R\}=D_5^2\left(\frac{1}{2}-\langle\tilde{T}_1\rangle\right)-D_5D_6(\langle\tilde{T}_2\rangle-\langle\tilde{T}_3\rangle)/2, \tag{3.22}$$

and we have written $\delta\omega_p'=(\Omega'+\delta)/2+\delta\omega$, where $\delta\omega$ is now the detuning from the center of the right feature.

IV. NUMERICAL RESULTS FOR PROBE ABSORPTION SPECTRA

Having available the analytical solutions for the Mollow and Autler-Townes spectra, we can discuss the dependence of the spectra on the bandwidth of the squeezed field applied to the system. With the central squeezing frequency equal to the laser frequency, there are three interesting cases to consider: the broad bandwidth, DPA, and NDPA narrow bandwidth. In order to compare the broadband and narrow band cases, the strong field regime $\Omega\gg\Gamma_0$ is treated, and various choices of the total phase ϕ are used. The Mollow spectra are calculated using Eq. (2.82) of I and the Autler-Townes spectra using Eq. (2.83) of I. Exactly the same numerical results are also obtained using the analytical forms Eqs. (3.7), (3.10), and (3.19) presented here.

All graphs used parameters $b_x=b_y$ for normal vacuum, $\{b_x=10,b_y=15\}$ for narrow bandwidth, and $\{b_x=600,b_y=900\}$ for broad bandwidth squeezed-vacuum field. In all cases the Rabi frequency $\Omega=100$. The Mollow absorption spectrum for the DPA source of the squeezed vacuum is plotted in Fig. 1 for the case of a narrow bandwidth squeezed-vacuum field. It is seen that the bandwidth of the

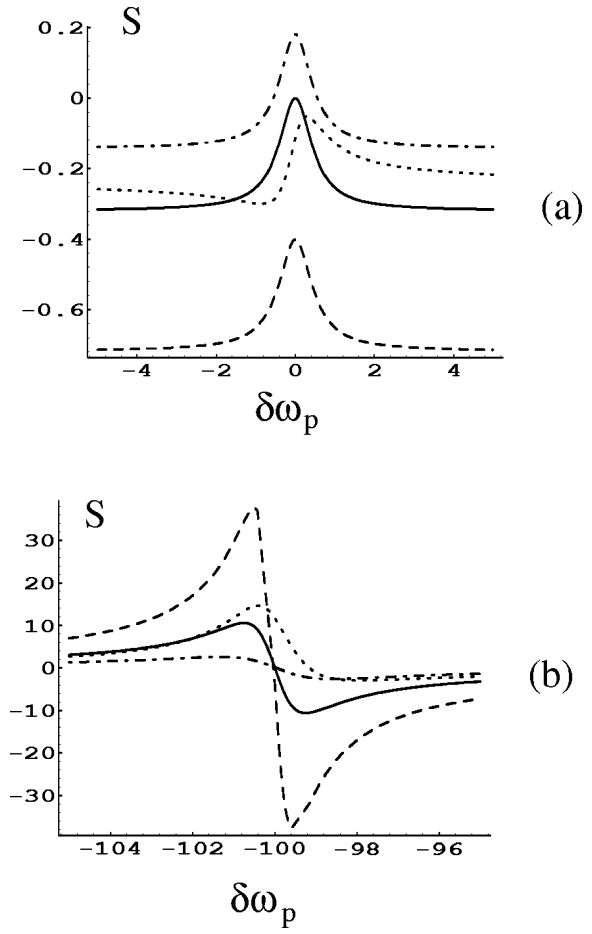

FIG. 1. Mollow probe absorption spectrum S (in units of Γ_0^{-1}) for the case of DPA versus probe detuning $\delta\omega_p$ (in units of Γ_0) in the case of resonance, $\delta=0$, and for a narrow bandwidth squeezed vacuum $b_x=10$, $b_y=15$. The Rabi frequency $\Omega=100$. The central component of the absorption spectrum is shown in (a), one of the Rabi sidebands in (b). The full line in the graphs represents the spectra in the absence of squeezed vacuum. Results for various ϕ are (i) $\phi=0$ (dashed line), (ii) $\phi=\pi/2$ (dotted line), (iii) $\phi=\pi$ (dot-dashed line). In all cases $\omega_s=\omega_a$.

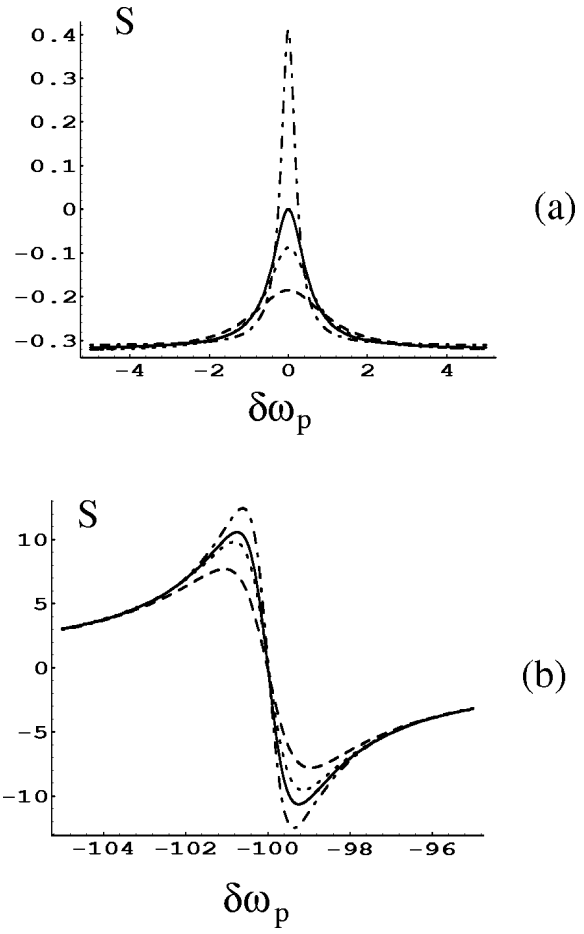

FIG. 2. Mollow probe absorption spectrum S (in units of Γ_0^{-1}) for the case of NDPA versus probe detuning $\delta\omega_p$ (in units of Γ_0) in the case of resonance, $\delta=0$, and for a narrow bandwidth squeezed vacuum $b_x=10$, $b_y=15$. The Rabi frequency $\Omega=100$. The central component of the absorption spectrum is shown in (a), one of the Rabi sidebands in (b). The full line in the graphs represents the spectra in the absence of squeezed vacuum. Results for various ϕ are (i) $\phi=0$ (dashed line), (ii) $\phi=\pi/2$ (dotted line), (iii) $\phi=\pi$ (dot-dashed line). In all cases $\omega_s=\omega_a$ and $\alpha=\Omega'$.

central component [Fig. 1(a)] is independent of the phase ϕ and is the same as in the ordinary vacuum. The amplitude of the feature depends on the phase and changes from absorptionlike for $\phi=0$ and π to dispersionlike as the phase changes to $\phi=\pi/2$. The bandwidth of the Rabi sidebands [Fig. 1(b)], however, depends on the phase ϕ and for $\phi=0$ the sidebands can be significantly narrowed compared to that in the normal vacuum.

In Fig. 2, we plot the Mollow spectrum for the NDPA source of the narrow bandwidth squeezed-vacuum field. In this case the central line is absorptive for all values of ϕ, but for $\phi=\pi$ can be narrower than that in the normal vacuum. The Rabi sidebands exhibit a weak dependence on the phase ϕ and for $\phi=\pi$ can be narrower than that in the normal vacuum. The narrowing, however, is small.

Figure 3 shows the Mollow absorption spectrum for the broadband squeezed vacuum field. The central line [Fig. 3(a)] exhibits exactly the same dependence on the phase as in the NDPA case [see Fig. 2(a)]. The Rabi sidebands are always broadened independent of the phase ϕ.

The left feature of the Autler-Townes absorption spectrum is shown in Fig. 4 for different types of the squeezed-vacuum field. For the DPA source [Fig. 4(a)] of the squeezed vacuum and $\phi=0$ the feature can be narrower than that in the normal vacuum. For the NDPA [Fig. 4(b)] the narrowing is observed for $\phi=\pi$. In the broadband case [Fig. 4(c)], however, the feature is always broadened independent of the phase ϕ. The same conclusion applies for the right feature.

V. THE BANDWIDTHS OF THE SPECTRAL FEATURES

A. Mollow spectrum

In order to get a better insight into the effects of a squeezing bandwidth on the spectral features, we evaluate analytical formulas for the bandwidths of the spectral features. From Eq. (3.7), the bandwidth Γ_C at the central feature of the Mollow probe absorption spectrum is given by $2H_1$.

For a narrow bandwidth DPA source of the squeezed field, the damping parameters $\tilde{M}(\omega_i)$ and $\tilde{\Gamma}_N(\omega_i)$ are given

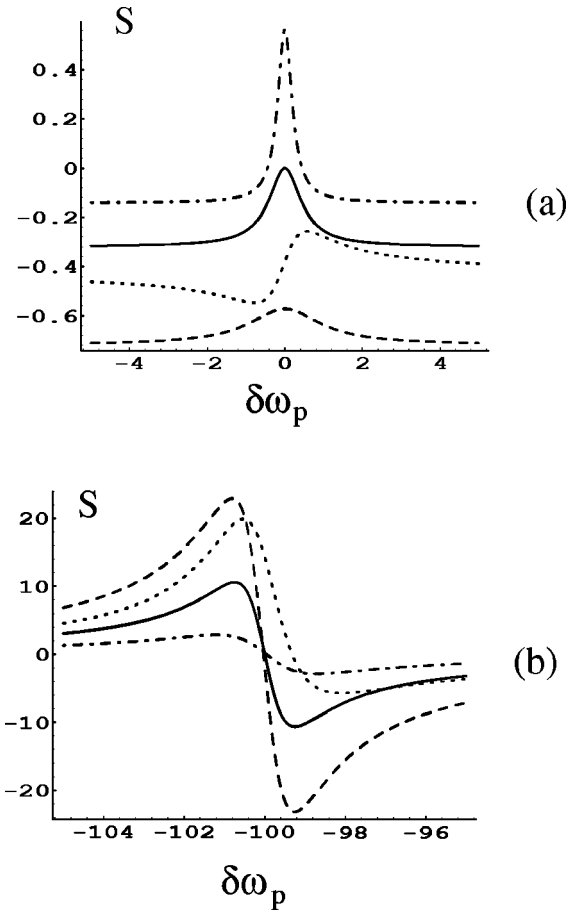

FIG. 3. Mollow probe absorption spectrum S (in units of Γ_0^{-1}) for the case of broad bandwidth squeezed vacuum ($b_x=600$, $b_y=900$) versus probe detuning $\delta\omega_p$ (in units of Γ_0) in the case of resonance, $\delta=0$. The Rabi frequency $\Omega=100$. The central component of the absorption spectrum is shown in (a), one of the Rabi sidebands in (b). The full line in the graphs represents the spectra in the absence of squeezed vacuum. Results for various ϕ are (i) $\phi=0$ (dashed line), (ii) $\phi=\pi/2$ (dotted line), (iii) $\phi=\pi$ (dot-dashed line). In all cases $\omega_s=\omega_a$.

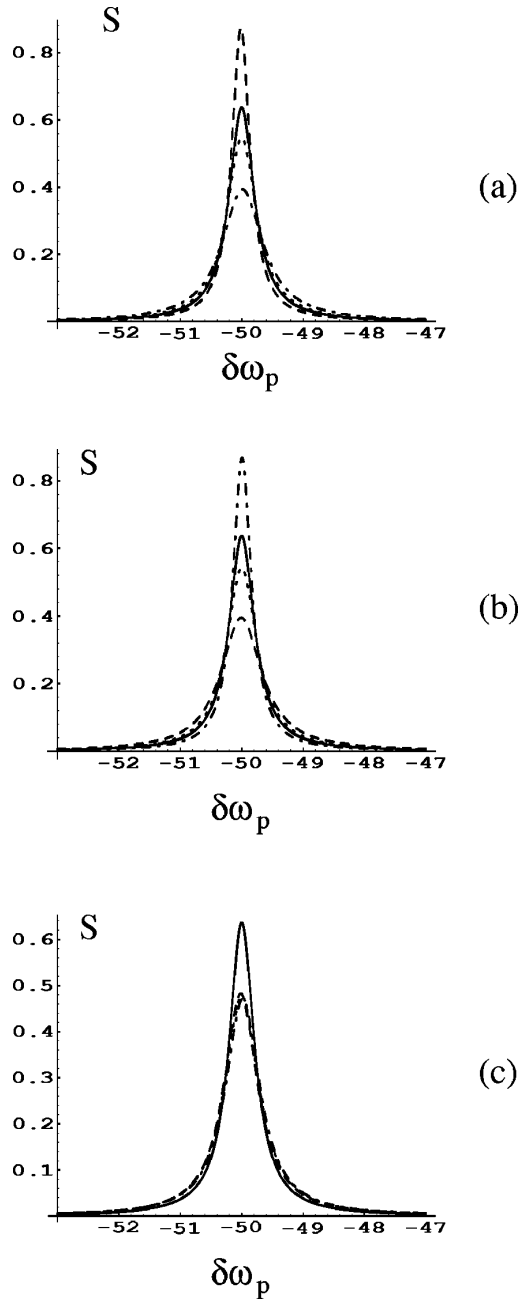

FIG. 4. Autler-Townes probe absorption spectrum S (in units of Γ_0^{-1}) for the narrow bandwidth squeezed-vacuum cases DPA (a), NDPA (b), and broadband squeezed vacuum (c) versus probe detuning $\delta\omega_p$ (in units of Γ_0) in the case of resonance, $\delta=0$. In (a) and (b) $b_x=10$ and $b_y=15$ and in the case (c) $b_x=600$ and $b_y=900$. In all cases $\Omega=100$. The full line in the graphs represents the spectra in the absence of squeezed vacuum. Results for various ϕ are (i) $\phi=0$ (dashed line), (ii) $\phi=\pi/2$ (dotted line), (iii) $\phi=\pi$ (dot-dashed line). In all cases $\omega_s=\omega_a$ and $\alpha=\Omega'$ for NDPA.

in Eq. (2.18). Applying Eq. (2.18) to H_1, given in Eq. (3.3), we find that

$$\Gamma_C=2(D_2^2+D_3^2)\Gamma_0. \tag{5.1}$$

Hence, the bandwidth of the central feature for the DPA case is independent of the squeezing parameters as is seen in Fig. 1 and is the same as in the ordinary vacuum. Note that $D_2=D_3=1/2$ for $\delta=0$.

For a narrow bandwidth NDPA source of the squeezed field, the parameters $\tilde{M}(\omega_i)$ and $\tilde{\Gamma}_N(\omega_i)$ are given in Eq. (2.19), and in this case we obtain

$$\Gamma_C=2(D_2^2+D_3^2)\Gamma_0+4N\Gamma_0-8D_2D_3(N-M\cos\phi)\Gamma_0. \tag{5.2}$$

The first term corresponds to the normal vacuum bandwidth, the second term is always positive, and the third term can be positive or negative depending on the phase ϕ. This effect is seen in Fig. 2. The bandwidth Γ_C now depends on the squeezing parameters and the detuning δ. For $N\to\infty$ and $\phi=\pi$, the bandwidth reduces to

$$\Gamma_C=2(D_2-D_3)^2\Gamma_0+4N(1-4D_2D_3)\Gamma_0, \tag{5.3}$$

which for $\delta\neq0$ is always greater than the bandwidth in the normal vacuum. However, for $\delta\to0$, $D_2, D_3\to1/2$ and then $\Gamma_C\to0$, indicating that for a resonant driving field and $N\to\infty$ the bandwidth of the central feature can be completely

suppressed. In practice, this limit can be well approached even with relatively small values of N. For example, with $N=1$ the bandwidth for the central feature is about $0.17\Gamma_0$.

Now, we consider a broad bandwidth squeezed vacuum. In this case the expressions for $\tilde{M}(\omega_i)$ and $\tilde{\Gamma}_N(\omega_i)$ are independent of ω_s and are given by

$$\tilde{M}(\omega_i)=-\frac{\Gamma_0}{2}e^{2i\phi}M,$$

$$\tilde{\Gamma}_N(\omega_i)=(1+2N)\Gamma_0. \tag{5.4}$$

Substituting these into H_1 in Eq. (3.3), we find that the bandwidth of the central Mollow feature is

$$\Gamma_C=2(D_2^2+D_3^2)\Gamma_0+4N\Gamma_0-8D_2D_3(N-M\cos\phi)\Gamma_0. \tag{5.5}$$

Comparing with Eq. (5.2), we see that this is identical to the NDPA case. Again the phase response of the bandwidth is seen in Fig. 3.

From Eqs. (3.10) and (3.11), the bandwidth Γ_S of the Rabi sidebands of the Mollow probe absorption spectrum is given by $2|H_4|$, where H_4 is given in Eq. (3.3).

Applying functions $\tilde{M}(\omega_i)$ and $\tilde{\Gamma}_N(\omega_i)$ from Eq. (2.18), we find that for the narrow DPA source the bandwidth of the left and right features of the Mollow probe absorption features is

$$\Gamma_S=(1+2D_2D_3)\Gamma_0-2D_1^2(N-M\cos\phi)\Gamma_0. \tag{5.6}$$

Since $D_1^2=-4D_2D_3$, the narrowing of the feature is possible only for $\phi=0$. For $N\gg1$ and $\phi=0$ the bandwidth reduces to

$$\Gamma_S=(1-2D_2D_3)\Gamma_0, \tag{5.7}$$

which is narrower than that in the normal vacuum [$\Gamma_S=(1+2D_2D_3)\Gamma_0$]. Hence, in the DPA case the Rabi sidebands can be narrowed below the normal vacuum level for all values of the detuning δ. The maximum narrowing, however, appears for $N\gg1$ and $\delta=0$, where $\Gamma_C=1/2\Gamma_0$. Again this narrowing is readily achieved even with relatively small values of N. For $N=1$, the bandwidths of the Rabi sidebands are about $0.671\Gamma_0$, which is very close to $1/2\Gamma_0$. The narrowing of the sidebands predicted by the analytical results agrees perfectly with the numerical results (see Fig. 1).

For the NDPA case, we find after substituting the functions $\tilde{M}(\omega_i)$ and $\tilde{\Gamma}_N(\omega_i)$ from Eq. (2.19) into H_4 that the bandwidths of the Rabi sidebands are

$$\Gamma_S=(1+2D_2D_3)\Gamma_0+2N\Gamma_0-4D_2D_3(N-M\cos\phi)\Gamma_0. \tag{5.8}$$

In this case, the Rabi sidebands can be narrowed below the normal vacuum level only for $\delta=0$ and phase $\phi=\pi$. For $N\gg1$ and $\phi=\pi$ the bandwidth can be written as

$$\Gamma_S=\Gamma_0+2N(1-4D_2D_3)\Gamma_0. \tag{5.9}$$

Clearly, the bandwidth is independent of N and equal to Γ_0 only for $\delta=0$, where $4D_2D_3=1$. This bandwidth is smaller than that in the normal vacuum, where for $\delta=0$, $\Gamma_S=3/2\Gamma_0$. In practice, with $N=1$ the bandwidths of the Rabi sidebands are approximately $1.086\Gamma_0$, which is close to Γ_0. This result also agrees with the numerical result shown in Fig. 2(b).

Finally, substituting Eq. (5.4) into H_4, we obtain bandwidths of the sidebands for the broad bandwidth squeezed vacuum

$$\Gamma_S=(1+2D_2D_3)\Gamma_0+2N\Gamma_0+4D_2D_3(N-M\cos\phi)\Gamma_0. \tag{5.10}$$

Maximum narrowing can occur for $\delta=0$ and the phase $\phi=0$. Then the bandwidths of the Rabi sidebands are given by

$$\Gamma_S=\frac{3}{2}\Gamma_0+(3N-M\cos\phi)\Gamma_0. \tag{5.11}$$

Note that the first term correctly predicts the normal vacuum bandwidths in the case of resonance ($\delta=0$). For the phase $\phi=0$, the second term can be negative [36,37]. This happens for $0<N<1/8$, with the maximum negative value about $-0.086\Gamma_0$ for $N\approx0.0303$. Thus the narrowing of the Rabi sidebands in the case of broad bandwidth squeezed vacuum is very small. For $N\gg1$, the bandwidth (5.10) reduces to $(1+2N)\Gamma_0$ independent of the detuning δ. This broadening has been observed in our numerical results Fig. 3(b).

B. Autler-Townes spectrum

Now we analyze the bandwidths of the Autler-Townes spectrum. From Eqs. (3.19) and (3.21) we see that the bandwidths of the two lines of the Autler-Townes probe absorption spectrum are given by $2|H_9|$ and $2|H_6|$, respectively.

For the DPA case, the bandwidth of the left feature of the Autler-Townes probe absorption spectrum is given by

$$\Gamma_L'=D_2\Gamma_0+2D_2D_3(N-M\cos\phi)\Gamma_0. \tag{5.12}$$

The first term, $D_2\Gamma_0$, is the bandwidth in the normal vacuum and the second term is induced by the squeezed vacuum. The phase dependence indicates a larger bandwidth for $\phi=\pi$ than for $\phi=0$ and this is seen in Fig. 4(a). In the limit $N\to\infty$ and $\phi=0$, the bandwidth of the feature goes to $D_2^2\Gamma_0$, which is much smaller than the bandwidth $D_2\Gamma_0$ in the normal vacuum. It is interesting to note that the bandwidth of the left feature can be reduced below the normal vacuum value for all positive detunings δ ($\delta>0$). Similarly, the right feature in the DPA case is given by

$$\Gamma_R'=D_3\Gamma_0+2D_2D_3(N-M\cos\phi)\Gamma_0. \tag{5.13}$$

For $N\to\infty$ and $\phi=0$ the bandwidth goes to $D_3^2\Gamma_0$, which is much smaller than the bandwidth $D_3\Gamma_0$ in the normal vacuum. Therefore, the bandwidth of the right feature can be reduced below the normal vacuum value for all negative detunings δ ($\delta<0$). The numerical results are in agreement with this result [see Fig. 4(a)].

In the NDPA case, the bandwidth of the left feature of the Autler-Townes probe absorption spectra is given by

$$\Gamma_L' = D_2\Gamma_0 + N\Gamma_0 - 2D_2D_3(N - M\cos\phi)\Gamma_0. \quad (5.14)$$

In this case the linewidth is smaller for $\phi=\pi$ compared to $\phi=0$ and this is seen in Fig. 4(b). For $\phi=\pi$ and $N\to\infty$, Γ_L' reduces to

$$\Gamma_L' = D_2(1-D_3)\Gamma_0 + N(1-4D_2D_3)\Gamma_0. \quad (5.15)$$

In this case the linewidth is broadened for $\delta\neq 0$. Only for $\delta=0$, where $4D_2D_3=1$, the linewidth can be reduced below the normal vacuum value, where the narrowing from $1/2\Gamma_0$ to $1/4\Gamma_0$ is observed. Similarly, the right feature in the NDPA case is given by

$$\Gamma_R' = D_3\Gamma_0 + N\Gamma_0 - 2D_2D_3(N - M\cos\phi)\Gamma_0, \quad (5.16)$$

where the left feature can be reduced to $1/4\Gamma_0$ only for $\delta=0$.

In the broad bandwidth regime, substituting the expressions for $\tilde{M}(\omega_i)$ and $\tilde{\Gamma}_N(\omega_i)$ from Eq. (5.4), the bandwidths of the Autler-Townes probe absorption features are given by

$$\Gamma_L' = (D_2+N)\Gamma_0,$$

$$\Gamma_R' = (D_3+N)\Gamma_0, \quad (5.17)$$

which are always broadened compared to that in the normal vacuum independent of the squeezing correlations and the phase. The lack of phase dependence of the linewidth is seen in Fig. 4(c). A similar result has also been found by Jakob and Kryuchkyan [38].

Hence, the linewidths of the Autler-Townes probe absorption spectrum depend on the squeezing correlations and the phase only in a narrow-bandwidth squeezed vacuum. Equations (5.14)–(5.17) show that the narrowing of the Autler-Townes spectral lines is intrinsically the narrow-bandwidth effect and does not extend to the broadband case.

VI. SUMMARY

We have considered the Mollow and Autler-Townes probe absorption spectra, of a three-level atom in a cascade configuration, with the lower transition coherently driven and coupled to the squeezed-vacuum field.

Analytical expressions for the spectra were obtained for the squeezed-vacuum frequency ω_s equal to the driving frequency ω_a and compared with the numerical results. The NDPA and the broadband squeezed-vacuum fields both lead to the narrowing of the central feature of the Mollow probe absorption spectra, and in the limit $N\to\infty$ the bandwidth of the feature can be reduced to zero. At the sidebands, a large narrowing is possible only with the DPA source of the squeezed vacuum. Broad bandwidth source only leads to a broadening of the Rabi sidebands except for $0<N<1/8$, when a very small narrowing is possible. The Autler-Townes probe absorption spectrum depends on the phase only for a narrow bandwidth squeezed vacuum, for both the DPA and NDPA sources. We have found that for a broadband squeezed vacuum the spectrum is independent of the phase and the spectral lines are always broadened compared to that in the normal vacuum.

ACKNOWLEDGMENTS

The authors wish to thank S.M. Barnett, M.R. Ferguson, and S. Swain for helpful discussions. One of us (Z.F.) is grateful to the Australian Research Council for support.

[1] C. W. Gardiner, Phys. Rev. Lett. **56**, 1917 (1986).
[2] A. S. Parkins, *in Modern Nonlinear Optics*, edited by M. Evans and S. Kielich (Wiley, New York, 1993), Pt. II, p. 607.
[3] E. S. Polzik, J. Carri, and H. J. Kimble, Phys. Rev. Lett. **68**, 3020 (1992); Appl. Phys. B **55**, 279 (1992).
[4] N. Ph. Georgiades, E. S. Polzik, K. Edamatsu, H. J. Kimble, and A. S. Parkins, Phys. Rev. Lett. **75**, 3426 (1995).
[5] N. Ph. Georgiades, E. S. Polzik, and H. J Kimble, Phys. Rev. A **55**, R1605 (1997).
[6] S. Smart and S. Swain, Phys. Rev. A **48**, R50 (1993).
[7] S. Swain, Phys. Rev. Lett. **73**, 1493 (1994).
[8] S. Swain and P. Zhou, Phys. Rev. A **52**, 4845 (1995).
[9] S. Swain and P. Zhou, Opt. Commun. **123**, 310 (1996).
[10] Z. Ficek, W. S. Smyth, and S. Swain, Opt. Commun. **110**, 555 (1994).
[11] Z. Ficek, W. S. Smyth, and S. Swain, Phys. Rev. A **52**, 4126 (1995).
[12] P. Zhou, Z. Ficek, and S. Swain, J. Opt. Soc. Am. B **13**, 768 (1996).
[13] R. Vyas and S. Singh, Phys. Rev. A **45**, 8095 (1992).
[14] A. S. Parkins and C. W. Gardiner, Phys. Rev. A **37**, 3867 (1988).
[15] H. Ritsch and P. Zoller, Phys. Rev. Lett. **61**, 1097 (1988).
[16] H. Ritsch and P. Zoller, Phys. Rev. A **38**, 4657 (1988).
[17] G. Yeoman and S. M. Barnett, J. Mod. Opt. **43**, 2037 (1996).
[18] A. S. Parkins, Phys. Rev. A **42**, 6873 (1990).
[19] A. S. Parkins, Phys. Rev. A **42**, 4352 (1990).
[20] C. W. Gardiner and A. S. Parkins, Phys. Rev. A **50**, 1792 (1994).
[21] C. W. Gardiner, A. S. Parkins, and M. J. Collett, J. Opt. Soc. Am. B **4**, 1683 (1987).
[22] A. S. Parkins, P. Zoller, and H. J. Carmichael, Phys. Rev. A **48**, 758 (1993).
[23] C. Cohen-Tannoudji and S. Reynaud, J. Phys. B **10**, 345 (1977).
[24] H. J. Carmichael and D. F. Walls, J. Phys. A **6**, 1552 (1973).
[25] B. Piraux, R. Bhatt, and P. L. Knight, Phys. Rev. A **41**, 6296 (1990).
[26] J. Cresser, J. Mod. Opt. **39**, 2187 (1992).
[27] C. H. Keitel, P. L. Knight, L. M. Narducci, and M. O. Scully, Opt. Commun. **118**, 143 (1995).
[28] M. Bosticky, Z. Ficek, and B. J. Dalton, Phys. Rev. A **53**, 4439 (1996).
[29] M. R. Ferguson, Z. Ficek, and B. J. Dalton, J. Mod. Opt. **42**, 679 (1995).
[30] B. R. Mollow, Phys. Rev. A **5**, 2217 (1972).

[31] B. R. Mollow, Phys. Rev. A **5**, 1522 (1972).
[32] P. D. Drummond and M. D. Reid, Phys. Rev. A **41**, 3930 (1990).
[33] C. W. Gardiner and M. J. Collett, Phys. Rev. A **31**, 3761 (1985).
[34] M. J. Collett and C. W. Gardiner, Phys. Rev. A **30**, 1386 (1984); M. J. Collett, R. Loudon, and C. W. Gardiner, J. Mod. Opt. **34**, 881 (1987).
[35] M. Lax, Phys. Rev. **172**, 350 (1968).
[36] T. Quang, M. Kozierowski, and L. Lan, Phys. Rev. A **39**, 644 (1989).
[37] A. Banerjee, Phys. Rev. A **52**, 2472 (1995).
[38] M. Jakob and G. Yu. Kryuchkyan, Phys. Rev. A **57**, 1355 (1998).